Chemistry – A European Journal

ChemEurJ Chemistry Europe European Chemical Societies Publishing

RESEARCH ARTICLE OPEN ACCESS

Readily Accessible bTurea-Derived Nitroxide Polarizing Agents for Dynamic Nuclear Polarization: bcTCOOKs and bcTmols

Ancy T. Wilson[1] | Shubha S. Gunaga[2] | Frederic Mentink-Vigier[2,3] | Snorri Th. Sigurdsson[1]

[1]Department of Chemistry, Science Institute, University of Iceland, Reykjavik, Iceland | [2]National High Magnetic Field Laboratory, Florida State University, Tallahassee, Florida, USA | [3]Department of Chemistry and Biochemistry, Florida State University, Tallahassee, Florida, USA

Correspondence: Frederic Mentink-Vigier (fmentink@fsu.edu) | Snorri Th. Sigurdsson (snorrisi@hi.is)

Received: 17 April 2026 | **Revised:** 12 June 2026 | **Accepted:** 3 July 2026

Keywords: bTurea | DNP-NMR | Nitroxide Biradical | NMR Spectroscopy | Radicals

ABSTRACT

Dynamic nuclear polarization (DNP) enhances the sensitivity of solid-state nuclear magnetic resonance (ssNMR) by transferring polarization from unpaired electron spins to nuclear spins. In this work, two series of bTurea-based biradicals, named bcTmols and bcTCOOKs, were synthesized through short and practical routes. Variation in the *N*-alkyl substitution on the urea bridge affected the electron–electron interactions and the overall DNP efficiency. Conformer analysis was carried out using density functional theory (DFT) to identify the dominant conformers along with the *g*-tensor orientations, dipolar couplings, and exchange interactions, which correlate with their electron paramagnetic resonance (EPR) and DNP properties. The results show that methyl substitution on the urea bridge restricts conformational flexibility, leading to more stable geometries and improved DNP performance. Among all the radicals, bcTCOOK-M2 provided the highest overall synthetic yield (8.3%) and signal enhancement (ca. 220) with a buildup time of 3.9 s at 14.1 T and 100 K, making it competitive with AsymPol-POK, including measurements in proton-rich media. The combination of straightforward synthesis, good solubility in aqueous solvents, and conformational stability makes bcTCOOK-M2 a promising polarizing agent for modern magic angle spinning (MAS) DNP applications.

1 | Introduction

Solid-state nuclear magnetic resonance (ssNMR) spectroscopy with magic angle spinning (MAS) is an indispensable tool for investigating the structure and dynamics of molecules and materials (polymers, inorganic solids, etc.) in the solid state at the atomic level [1]. However, the inherent insensitivity of NMR, arising from the small energy involved in NMR (hundreds of MHz) versus the thermal energy (~5–10 THz for ^{1}H at room temperature), leads to low nuclear spin magnetization and precludes its use for many applications where the nuclear isotope is at low concentration [2]. Thus, enhancing the sensitivity of NMR spectroscopy opens up new analytical possibilities in various interdisciplinary fields, such as structural biology and materials science. Dynamic nuclear polarization (DNP) has emerged as a powerful technique to increase the sensitivity of NMR by transferring the higher magnetization of unpaired electrons (radicals) to nuclei of interest under microwave (μw) irradiation [3–6].

The signal enhancement of MAS DNP-NMR depends on the efficiency of the polarization transfer mechanisms, such as the solid effect (SE) [7–10], the cross effect (CE) [8, 9, 11–14], the Overhauser effect (OE) [15–18], and thermal mixing (TM) [6, 19–22]. Among these, the CE is recognized as the most effective mechanism in the solid state for polarization transfer at high

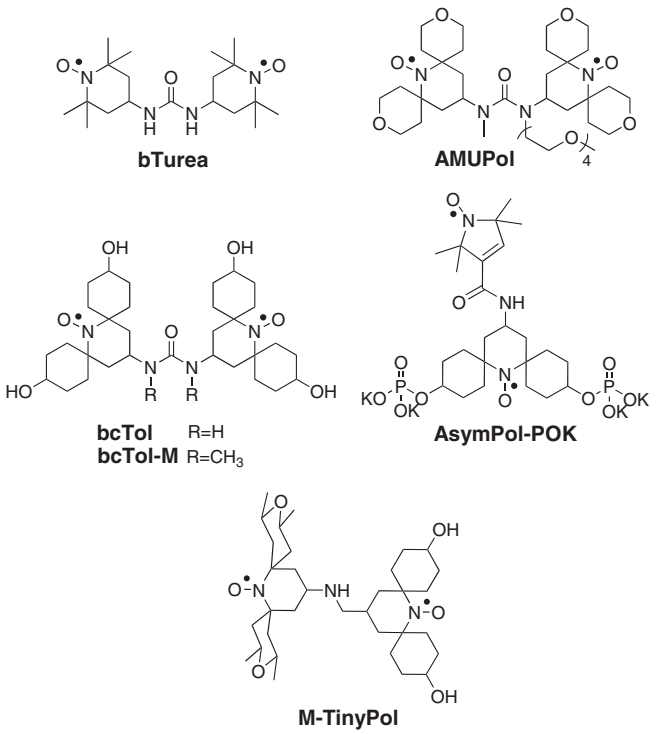

FIGURE 1 | Examples of nitroxide biradicals [24, 26, 27, 39, 41].

field (≥ 9.4 T), providing both large polarization gains and short polarization buildup times (T_B) [6, 8, 23, 24]. The basic model for the CE mechanism under MAS involves three spins, namely two electrons and one nucleus [8, 9, 25]; for CE to be active, the width of the EPR spectrum of the two coupled electron spins must encompass the nuclear Larmor frequency [8, 9, 25]. In practice, the CE mechanism is favored when using biradicals [9, 11, 25], which have become an important class of so-called polarizing agents. The design of efficient biradicals for DNP must take several factors into account, such as electron relaxation times, interelectronic distances, electron–electron and electronnuclei couplings, the relative orientation of the *g*-tensors of the electrons, as well as the conformational ensemble of biradicals [9, 23, 25–36].

Nitroxide-based biradicals have demonstrated remarkable DNP performance as polarizing agents, particularly at 9.4 and 14.1 T and 100 K [24, 26–29, 32, 37–42]. bTurea [37] (Figure 1) is an early biradical, in which two (2,2,6,6-tetramethylpiperidin-1-yl)oxyl (TEMPO) radicals were linked through a urea. This core structure was significantly improved by the inclusion of spirocycles [40, 43], leading to high DNP performance, and the addition of polar functional groups increased their solubility in aqueous solutions to meet the demands of structural biology [26, 27, 39, 41]. Examples include AMUPol [39], bcTol [41], and bcTol-M [26] (Figure 1). Other water-soluble biradicals with improved DNP performance have since been prepared, such as AsymPol-POK [24] and M-TinyPol (Figure 1) [27, 42]. In parallel, hetero-biradicals such as the trityl-nitroxides SNAPol [44], PyrroTriPol [45], and STAPol [46], as well as the BDPA-nitroxide HyTEK2 [47] have proven to be more efficient polarizing agents than bis-nitroxides at very high fields (≥ 16 T). Despite the high DNP performance offered by the aforementioned biradicals, their syntheses are non-trivial, which hinders their accessibility

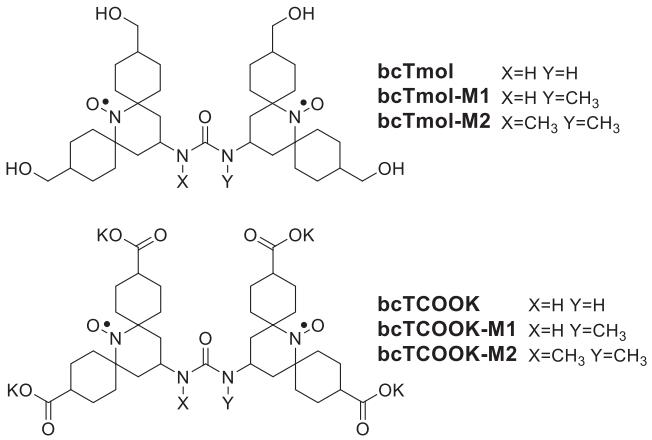

FIGURE 2 | Structures of the bcTmol and bcTCOOK derivatives.

due to the cost and time associated with biradical preparation. It is important to balance the ease of preparation and performance of biradicals for providing polarizing agents to the DNP community at large [48].

In this study, we describe the synthesis and DNP properties of two families of polarizing agents containing the bTurea core structure, the nonionic bcTmols and the ionic bcTCOOKs (Figure 2). The former has hydroxymethyl substituents on the spirocycles, while the latter has carboxylates. Within each subfamily, the number of methyl substituents on the nitrogen atoms in the urea linkage was varied, because such *N*-alkylations have been shown to change the conformational ensemble of bTurea-based biradicals [26, 28, 49, 50]. To provide a complete picture, the DNP performance of these biradicals was compared to the well-established biradicals bcTol, bcTol-M, and AsymPol-POK under identical experimental conditions.

2 | Results and Discussion

The aim of this study was to design and prepare high-performing bTurea-derived bis-nitroxides that were synthetically more easily accessible than other members of this family of polarizing agents. We used the key intermediate **1** [28] (Scheme 1A), which offers a simpler synthesis and purification process in comparison with the corresponding TBDMS-protected spirocyclohexanolyl ketone [26, 41], previously used for the synthesis of bcTol [41], bcTol-M [26], and AsymPol-POK [24]. Moreover, the diester **1** offers a divergent synthetic approach for the preparation of carboxylate derivatives (bcTCOOKs) and hydroxyl derivatives (bcTmols).

2.1 | Synthesis of bcTmols and bcTCOOKs

2.1.1 | The bcTmol Family

The synthesis of the bcTmols began with the reductive amination of **1** [28], with either CH_3NH_2·HCl or NH_4OAc, to obtain the amino derivatives **2** or **4** [28], respectively, in very good yields (Scheme 1A). The homocoupling of **2** with triphosgene, followed by reduction, yielded the *N,N*-dimethyl tetrahydroxyl derivative bcTmol-M2. Similarly, the self-coupling of **4** afforded

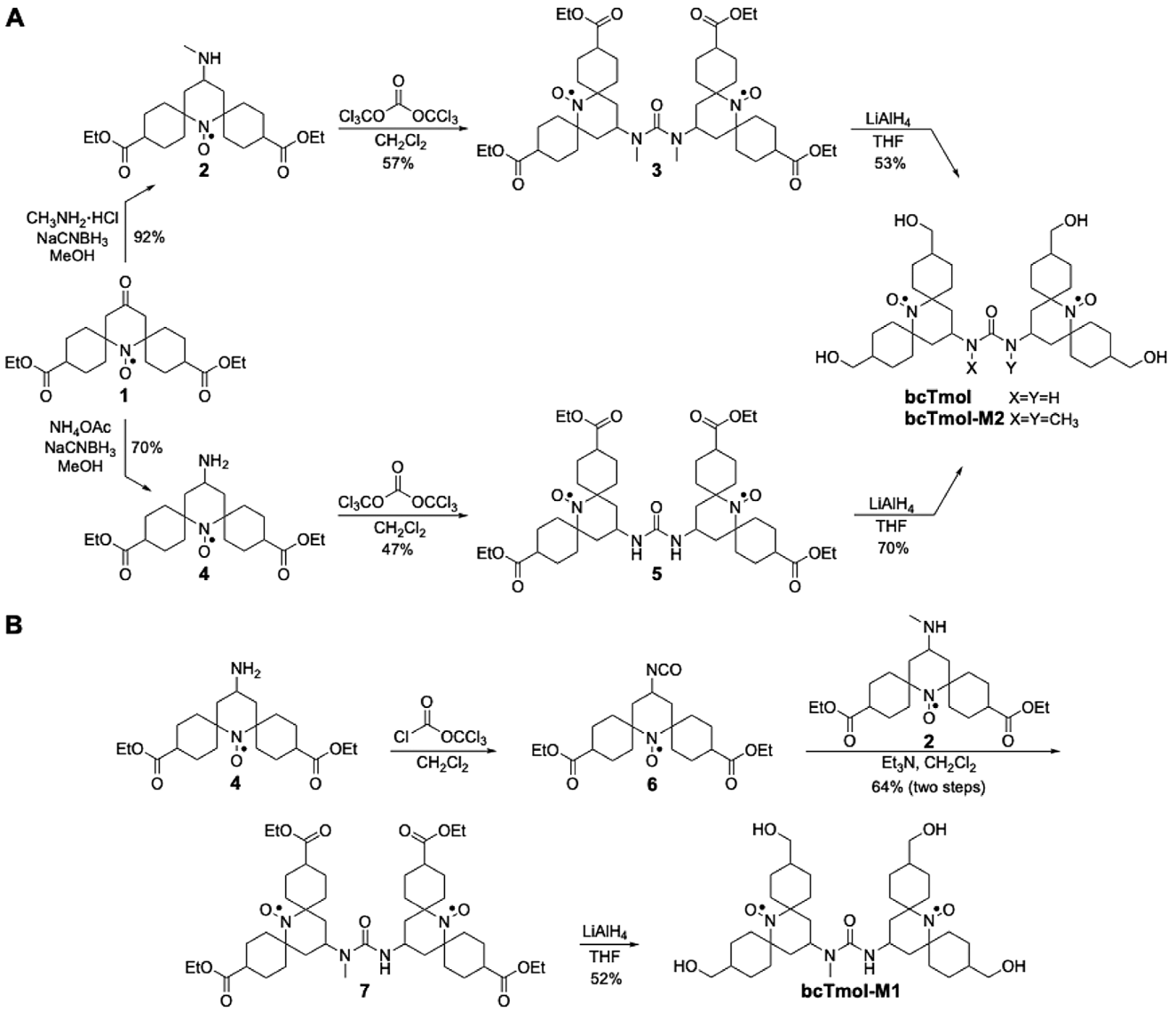

SCHEME 1 | (A) Synthesis of bcTmol, bcTmol-M2, and (B) bcTmol-M1.

urea derivative **5** [28], which on subsequent reduction yielded bcTmol. The synthesis of the asymmetric bcTmol-M1 utilized a different strategy (Scheme 1B). Diester amine **4** was reacted with diphosgene to yield the corresponding isocyanate **6**, followed by reaction with **2** to obtain *N*-methyl urea **7**. Reduction of **7** gave bcTmol-M1. The overall yield of bcTmol-M2 (6.4%) was significantly higher than the related bcTol-M (3.9%), bcTol (3.2%), and AsymPol-POK (2%). For bcTmol and bcTmol-M1, the overall yields were slightly lower than bcTmol-M2, namely 5.3% and 5.4%, respectively (Table S1).

2.1.2 | The bcTCOOK Family

The bcTCOOK derivatives were synthesized by hydrolysis of the corresponding tetraester ureas **5**, **7**, **3** under basic conditions, yielding bcTCOOK, bcTCOOK-M1, and bcTCOOK-M2, respectively (Scheme 2). Reverse-phase (RP) high-performance liquid chromatography (HPLC) analysis revealed three peaks for both bcTCOOK and bcTCOOK-M1, and four peaks for bcTCOOK-M2 (see Supporting Information). These peaks correspond to different isomers arising from the substitution of the spirocyclohexyl rings flanking the nitroxide moiety. Such isomers are also present in the bcTmols, but they were not as well resolved by RP-HPLC (see Supporting Information).

The products were desalted by RP-HPLC, affording good yields for bcTCOOK-M2 and moderate yields for bcTCOOK and bcTCOOK-M1. bcTCOOK-M2 was produced with an overall yield of 8.3%, substantially higher than previously reported bTurea derivatives (Table S1). In addition to improved yields, the synthetic procedures for the new derivatives are easier to implement than those previously reported for bcTol [41], bcTol-M [26], AsymPol-POK [24], and TinyPol [27]. In earlier synthesis, both the condensation and oxidation reactions using TBDMS-protected intermediates for the synthesis of the spirocyclohexanolyl nitroxide derivatives generated highly nonpolar side products with retention factor (R_f) values similar to those of the desired product [24]. This resulted in time-consuming chromatographic purifications, resulting in only 9% yield for the two steps.

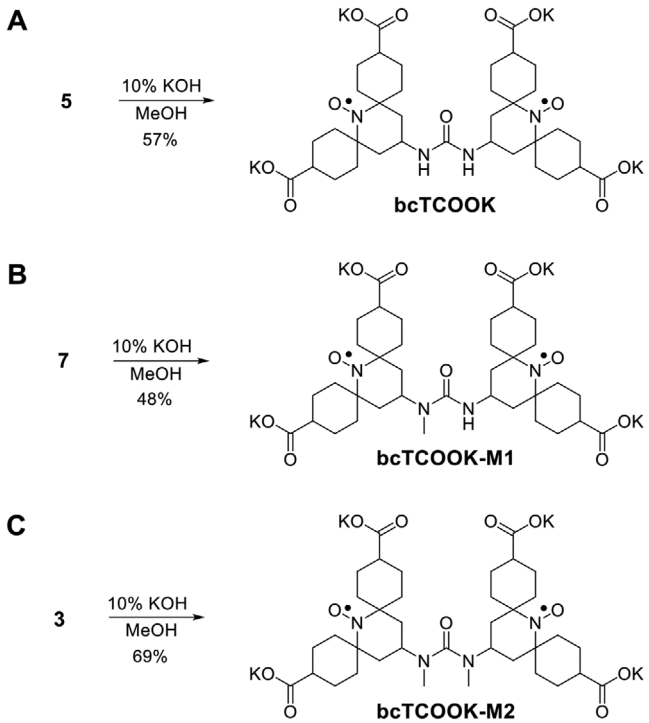

SCHEME 2 | (A) Synthesis of bcTCOOK, (B) bcTCOOK-M1, and (C) bcTCOOK-M2.

In contrast, the synthesis using ester-containing intermediate **1** circumvented the challenging purification steps associated with silyl-protected hydroxyls and side-reactions. Overall, the ester-based synthetic route adopted for the synthesis of bcTCOOK and bcTmol derivatives provided substantial improvements in terms of synthetic accessibility, ease of purification, and overall efficiency.

Since the intent was to use the bcTCOOKs and bcTmols for structural biology, their solubility in water was investigated. The bcTCOOKs were readily soluble (>3 M), while the bcTmols were only sparingly soluble (<2 mM), as determined by EPR spectroscopy (see Supporting Information). The low solubility of the bcTmols in water was surprising because the structurally similar bcTol and bcTol-M have solubilities of 100 mM [41] and 170 mM [26], respectively. Therefore, our main focus became the analysis and evaluation of the bcTCOOKs for MAS DNP-NMR.

2.2 | X-Band CW-EPR Spectra

Figure 3 shows the EPR spectra of the biradicals, recorded in water (left column) and MeOH (right column), along with the corresponding fits using EasySpin [51]. All the spectra possess the same attributes as previously reported spectra for bTureas, namely multiple lines (no less than 5), and shoulders at the extrema [28, 50]. Such features are characteristic of EPR spectra of biradicals in the intermediate coupling regime, where the nitrogen hyperfine coupling is greater or equal to the exchange interaction between the NO moieties [52]. Interestingly, there is a clear difference between the spectra recorded in water and MeOH: the transition at the far left of the EPR spectra (asterisks in Figure 3A) appears at lower magnetic field in water compared to MeOH (note that the same applies for the far-right transition), which indicates that the exchange interaction in water is stronger than in MeOH.

To go beyond visual inspection, we performed quantitative EPR simulations to determine the absolute values of the exchange interactions (Table 1). We initially tried fitting the spectra using a single exchange interaction, but the results were unsatisfactory (see Supporting Information). Better fits were obtained by considering two exchange interactions for MeOH and three for water. In all cases, the biradicals showed a mixture of coupling strengths: one fraction with weak exchange ($|J|$ <5 MHz in MeOH, or <8 MHz in water), and another with stronger exchange (~20–25 MHz). For water, a third fraction was needed, showing even higher exchange values (~30–40 MHz).

The weighted average exchange interaction increased from 11.2 to 15.6 MHz in MeOH, as the substitution on the urea bridge increased. A similar trend was observed for the spectra in water, starting from 17.3 for bcTCOOK and reaching 30.7 MHz for bcTCOOK-M2. The experimental trend, in either solvent, matches the previous characterization of bcTol, AMUPol, and bcTol-M in the solid state [50]. The substituents resulted in stronger exchange interaction for bcTol-M (J = −21 MHz) than for AMUPol (J = −15 MHz) and bcTol (J = −9 MHz). The DFT simulations appear to appropriately quantify the order of magnitude of the exchange interaction (*vide infra*).

Overall, the EPR measurements indicate that increasing the substitution on the urea bridge leads to better relative orientation and stronger exchange interactions. It should be noted that fits of the solid-state EPR spectra of these biradicals should optimally be obtained as previously done for other nitroxide biradicals [30, 32, 50, 53]. However, due to the numerous isomers/conformers that are possible, the task of fitting is bound to yield values that have little meaning as the number of fitting parameters exceeds the information contained in multiple fields. At best, it appears reasonable to assume that the experimental Euler angles and exchange interactions will be similar to those previously determined [50].

2.3 | In silico Structures of the bcTCOOKs

Before determining the DNP performance of the bcTCOOK biradicals, their structures were predicted using a multistep DFT process (see Supporting Information) to better understand their magnetic properties. In brief, we first screened the conformers using the extended tight binding method [54, 55]. From there, the lowest energy conformers were subjected to an additional DFT optimization, and the magnetic properties were computed for the best conformers (see Supporting Information for details).

As mentioned above, the bcTCOOKs contained isomers, originating from the configuration of the carbon on the spirocycles bearing the COOK substituent. This substituent prefers an equatorial position on the chair conformation of the cyclohexane ring. Depending on the configuration of the carbon bearing the substituent, the cyclohexyl ring favors either a

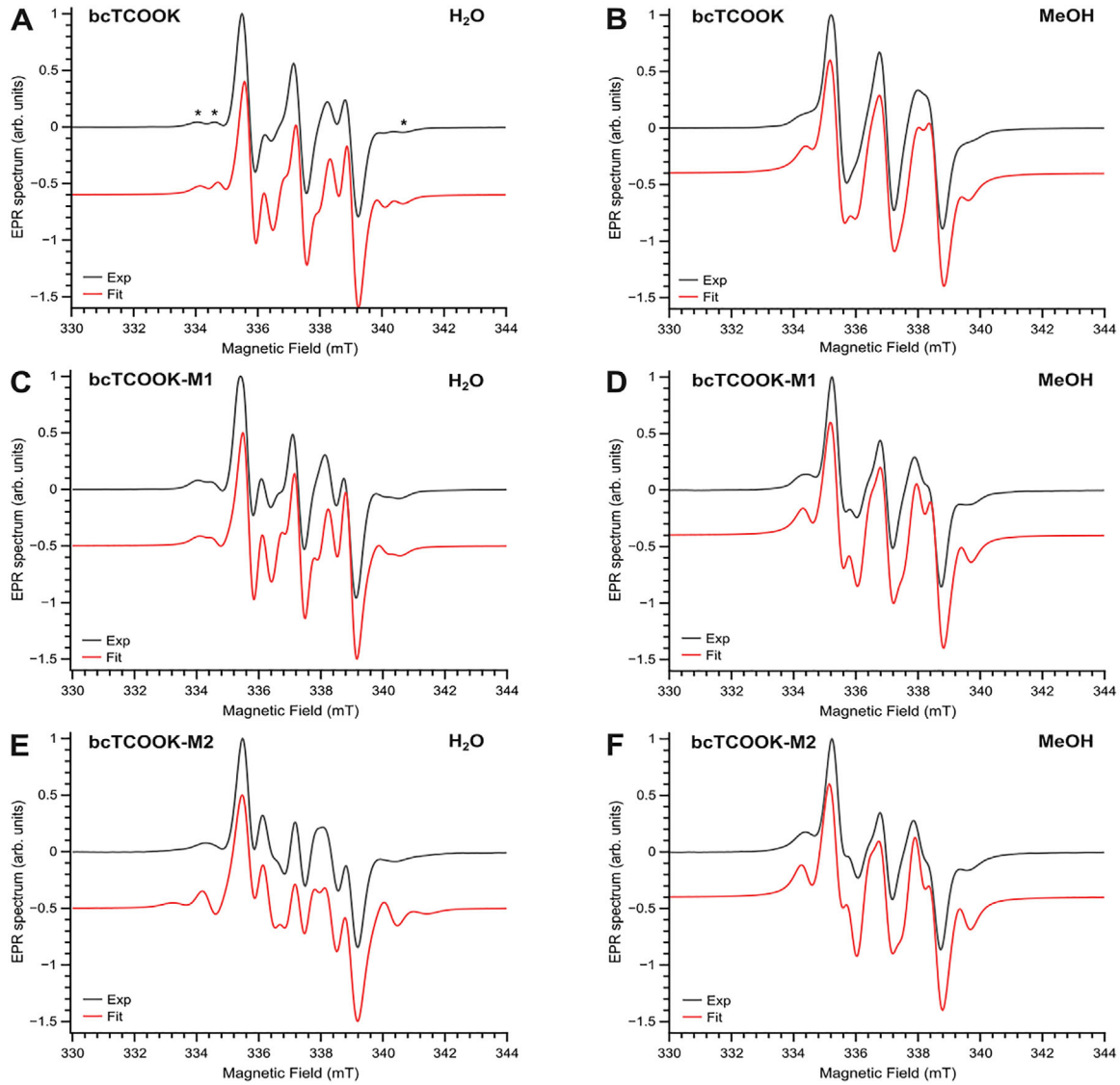

FIGURE 3 | X-band EPR spectra of bcTCOOK derivatives at 22°C. Top, (A) bcTCOOK in water and (B) in MeOH. Middle, (C) bcTCOOK-M1 in water, and (D) MeOH. Bottom, (E) bcTCOOK-M2 in water and (F) MeOH. The experimental spectra are black and the simulated spectra are red. The far left and right EPR transitions in A are marked with asterisks.

TABLE 1 | Exchange interaction and relative contribution obtained from fitting of the EPR spectra. The exchange interaction is according to the Hamiltonian convention $H_J = 2|J|S_1S_2$.

Biradical	Exchange interaction in water	Exchange interaction in MeOH
bcTCOOK	$\|J\|$ = 30 MHz (30%), 20 MHz (38%), and <2 MHz (38%); average: 17.3 MHz	$\|J\|$ = 20 MHz (50%) and 2.5 MHz (50%); average: 11.2 MHz
bcTCOOK-M1	$\|J\|$ = 30 MHz (30%), 22.5 MHz (38%), and <2 MHz (38%); average: 19.6 MHz	$\|J\|$ = 20 MHz (63%) and 2.5 MHz (37%); average: 13.5 MHz
bcTCOOK-M2	$\|J\|$ = 41 MHz (40%), 27 MHz (50%), and <8 MHz (10%); average: 30.7 MHz	$\|J\|$ = 20 MHz (71%) and 5 MHz (29%); average: 15.6 MHz

conformation that brings the ring close to the nitroxide (referred to as the "closed" conformation) or away from the nitroxide (the "open" conformation) [29, 42, 50, 56]. Figure S1 shows the major conformations of the three diastereomers of intermediate **4**, namely the open–open (oo), the open–closed (oc), the closed–open (co), and the closed–closed (cc) conformers. Since the isomer that favors the cc conformer is formed in small amounts [29] and because we only see two major peaks in the HPLC trace (see Supporting Information), we have not included it in our analysis. Consequently, the biradicals can adopt combinations,

TABLE 2 | Magnetic properties of bcTCOOK, bcTCOOK-M1, and bcTCOOK-M2 biradicals as predicted by DFT. The experimental values for bcTol [50], AMUPol [50], and bcTol-M [50] are listed for comparison. Weighted average was used for isomer combinations. The *g*-tensor distance is obtained as the Frobenius norm of the difference of the *g*-tensors; the exchange interaction according to the Hamiltonian convention $H_J = -2JS_1S_2$. Values have been averaged with respect to all conformers and isomers. On average, the principal values of the *g*-tensor are $[g_{xx}, g_{yy}, g_{zz}] = [2.0095, 2.0061, 2.0021]$. DFT simulations for the exchange interaction are very sensitive to the relative orientation [57], which can explain the underestimation with respect to the experiment.

Biradical	Predicted *g*-tensor relative orientation [α, β, γ] (degrees)	*g*-tensor distance (L, $\times 10^{-3}$)	Dipolar coupling (D, MHz)	Exchange interaction (J, MHz)
bcTCOOK	[65.92, 55.96, 112.13]	5.60 (1.2)	35.3 (0.2)	−8.20 (8.3)
bcTCOOK-M1	[58.74, 49.16, 125.93]	6 (1.6)	36.5 (0.9)	−12.9 (9.0)
bcTCOOK-M2	[57.60, 91.37, 115.42]	7.57 (0.5)	37.45 (0.7)	−9.90 (3.3)
bcTol	[67, 56,120] ± [10,10,5]	5.8	34 ± 1	−14 ± 1.5
AMUPol	[58, 57, 126] ± [5,10,5]	6.4	35 ± 2	−16 ± 2
bcTol-M	[58, 81,134] ± [5,10,10]	7.2–7.8	36 ± 2	−21 ± 2

such as oo–oo, oc–oo, and co–oo, where the dash denotes the urea bridge. In total, nine possible combinations exist, some of which are equivalent by symmetry. For each combination, the magnetic properties of the predominant conformers—typically two—were calculated, resulting in many simulations.

To compare the relative orientations between the different isomers/conformers, we used the term "distance between the *g*-tensors of electron spin 1 and 2", $||\hat{g}_1 - \hat{g}_2||_{Fro}$ [31]. This distance is a measure of how different the orientation of the main axis of one *g*-tensor is relative to the other (relates to the relative Euler angles), which depends on the relative spatial arrangements of the two nitroxides. It has been demonstrated that this distance correlates with the performance of the biradicals as a polarizing agent [50] and the higher the value, the better the expected DNP performance, the faster the buildup time, all other variables remaining identical. The predictions for all isomers/conformers are reported in Table S2. For simplicity, we only report the conformer-weighted average values in Table 2 and use them to discuss the properties.

For bcTCOOK, the four isomers exhibit only modest variations in magnetic properties. The different conformers span ranges of 1.2×10^{-3} for *g*-tensor distance, 0.2 MHz for dipolar coupling, and 8.3 MHz for exchange interaction (Table S2). These numbers quantify how much the oc conformer can influence DNP performance, outside of solubility variations. Averaged across all isomers, the predicted magnetic parameters generally align with experimental values reported for bcTol [50]. A similar trend is observed for bcTCOOK-M1; its average *g*-tensor distance, dipolar coupling, and exchange interaction agree well with AMUPol experimental data [50]. However, the M1 conformers exhibit a wider spread (e.g., 1.6×10^{-3} *g*-tensor distance and 9 MHz exchange interaction) than for bcTCOOK, suggesting greater flexibility and potential variability in performance. bcTCOOK-M2 possesses properties similar to bcTol-M [50], with a higher predicted *g*-tensor distance. However, the predicted exchange interaction is weaker than for bcTol-M, which is a likely consequence of DFT inaccuracy. Importantly, the M2 structure is rigid, making its magnetic properties insensitive to the presence of oc isomers. The variation across its isomers is significantly lower (exchange interaction spanning 3 MHz; *g*-tensor distance: 0.5×10^{-3}) than for the other compounds. Overall, this stability highlights that the "locking" mechanism induced by the methyl substituents on the urea bridge is an important and beneficial structural feature for maintaining predictable magnetic behavior. In summary, the in silico evaluation allows pre-ranking of the DNP performance of the biradicals: bcTCOOK is expected to perform worse than bcTCOOK-M1 and bcTCOOK-M2.

2.4 | DNP Performance

2.4.1 | The bcTCOOK Family

The water-soluble biradicals (bcTCOOK, bcTCOOK-M1, and bcTCOOK-M2), as well as a commercial batch of reference biradical AsymPol-POK [24], were evaluated in the standard glycerol-d_8/D_2O/H_2O mixture (6:3:1 *v*/*v*). Each sample was degassed by freeze-thaw cycles until the polarization buildup time was stabilized. The resulting DNP enhancements ($\epsilon_{on/off}$), the characteristic buildup time, the sensitivity and signal intensity are shown in Figure 4. The enhancement was 180, 160, and 220 for bcTCOOK, bcTCOOK-M1, and bcTCOOK-M2, respectively. Notably, bcTCOOK outperformed its predecessor bcTol in terms of enhancement (180 vs. 150) [50].

The characteristic hyperpolarization buildup time is a critical measure of DNP performance of samples that are challenging to hyperpolarize; the lower the value, the higher the DNP performance [23, 32, 58, 59]. Across the bcTCOOK series, buildup time decreased with increasing substitution on the urea bridge, from 6.6 s for bcTCOOK to 3.9 s for bcTCOOK-M2, highlighting the beneficial impact of structural modifications on polarization kinetics. These values are consistent with previous reports on bTurea derivatives featuring similar bridge substitutions [50].

Enhancement and buildup time are not the only measures of nuclear spin hyperpolarization efficiency, as it is also influenced by depolarization mechanisms that can vary across different experimental conditions and sample environments [60, 61]. Therefore, several research groups have begun using the

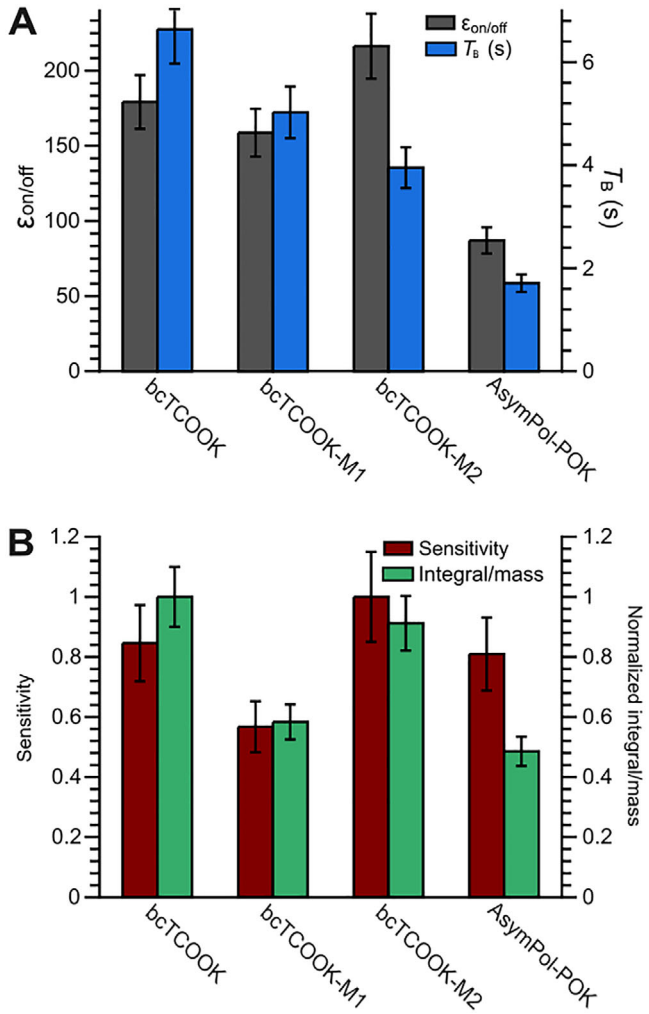

FIGURE 4 | DNP performance of the bcTCOOK family and AsymPol-POK (10 mM, glycerol-d_8/D_2O/H_2O (6:3:1 *v*/*v*)) at 14.1 T and 100 K. (A) The enhancement ($\epsilon_{on/off}$) and the buildup time (T_B). (B) Sensitivity and normalized integrals. Normalized integral/mass refers to the integrated NMR signal, divided by the mass of the sample packed in the rotor, allowing comparison of the absolute signal obtained per unit mass across samples. The sensitivity is normalized to the highest value. The measurement uncertainties were estimated in the order of ±10%, similarly to what has been reported by Wei et al. [33]; this leads to an uncertainty for the sensitivity of 15%.

signal-to-noise per square root of unit time (during μw irradiation) to objectively compare the DNP performance of different radicals [33, 41, 62–66]. This gives a true measure of the increase in sensitivity, defined as $S = I_{on} / \sqrt{T_B}$, where I_{on} is the NMR signal intensity with μw irradiation and T_B is the buildup time (all other parameters being constant), reported for the bcTCOOKs in Figure 4B. The sensitivity follows a similar trend as the enhancement, with bcTCOOK-M2 outperforming the others.

The high performance of bcTCOOK-M2 was anticipated based on the DFT calculations and the previous results obtained for bcTol-M (220 vs. 205) [50]. The performance can be explained by the better relative orientation that enables the cross-effect mechanism to be more efficient [25, 31, 34, 50]. Such optimal orientation favors larger polarization difference and thus, reaches values of enhancement closer to theoretical maximum [31, 50]. Additionally, stronger electron–electron coupling contributes to a faster polarization buildup time [8, 23, 58]. Thus, the outstanding performance of bcTCOOK-M2 is due to a combination of good relative orientation and a sizable dipolar/exchange interaction. In contrast, AsymPol-POK exhibits a less favorable average relative orientation with a *g*-tensor distance of only 5.3×10^{-3} [32]. This reduced *g*-tensor distance corresponds to a relative orientation that does not maximize hyperpolarization levels [31], thereby limiting both the electron spin polarization difference and, consequently, the maximum achievable nuclear spin hyperpolarization. However, this limitation is offset by its strong electron–electron coupling within AsymPol-POK (evidenced by dipolar coupling of 56 MHz and *J* exchange values of 100 and 120 MHz for each conformer) [32]. This high electron–electron coupling allows the biradical to achieve significantly faster buildup times. Ultimately, this trade-off—where a lower intrinsic hyperpolarization level (*g*-tensor distance) is compensated by accelerated kinetics (*D* and *J*)—enables AsymPol-POK to maintain overall high performance.

To evaluate the DNP performance of bcTCOOK-M2 under more demanding conditions, we tested it in a medium with a higher concentration of protons ($[^1H]$ = 66 M, glycerol/D_2O (6:4 v/v)), known to be challenging for bTurea-based polarizing agents such as AMUPol (Figure 5) [32, 33, 67]. Such high proton concentration is particularly relevant for biological samples and has previously been shown to reduce DNP efficiency, due to increased relaxation rates and unfavorable biradical-to-proton ratio. Interestingly, the enhancement of bcTCOOK-M2 is relatively unaffected (Figure 5). However, the buildup time is longer (~6 s), as previously observed for AMUPol, both at 9.4 T [67] and 14.1 T [32, 33, 67]. On the other hand, the buildup time (1.7 s) and enhancement (~100) of AsymPol-POK is similar. Thus, AsymPol-POK surpasses bcTCOOK-M2 by a modest 20% in sensitivity, which is close to the experimental uncertainty (Figure 5B). These differences are expected to be more significant as the proton concentration increases or when the intrinsic relaxation times of the protons become shorter, especially at high field. Indeed, the effect of proton concentration on DNP performance of derivatives of bTureas is more significant than for AsymPol [58]. However, bcTCOOK-M2 is still a very attractive biradical, particularly at lower field (e.g., 9.4 T), where we expect higher efficiency [23, 58].

2.4.2 | The bcTmol Family

Since the bcTmols had a very limited solubility in water, the DNP performance of bcTmol-M1 and bcTmol-M2 was evaluated in ethylene glycol/water (3/7 *v*/*v*) using a biradical concentration of 10 mM. This matrix forms a good glass but may be more challenging to hyperpolarize due to the larger proton concentration. As observed for the bcTCOOKs, the dimethyl derivative bcTmol-M2 provides higher enhancements (70 vs. 25) (Figure 6A) and higher sensitivity by a factor of ~2, compared to bcTmol-M1 (Figure 6B).

3 | Conclusion

We have described straightforward syntheses of two series of polarizing agents in the bTurea family, bcTCOOKs and bcTmols,

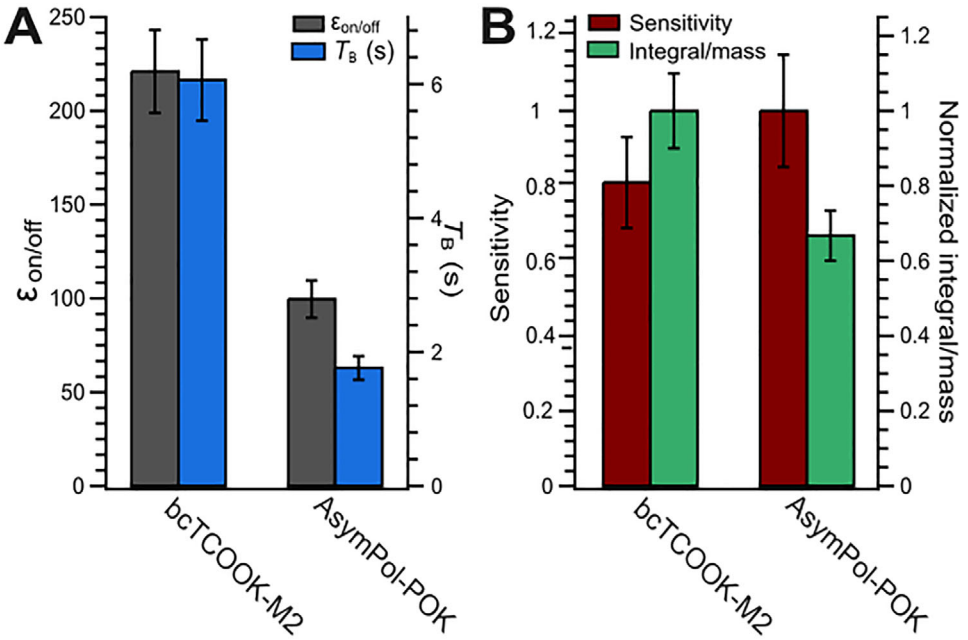

FIGURE 5 | DNP performance of bcTCOOK-M2 and AsymPol-POK in (10 mM, glycerol/D_2O (6/4 *v*/*v*)) at 14.1 T and 100 K. (A) The enhancement ($\epsilon_{on/off}$) and the buildup time (T_B). (B) Sensitivity and normalized integrals. Normalized integral/mass refers to the integrated NMR signal, divided by the mass of the sample packed in the rotor, allowing comparison of the absolute signal obtained per unit mass across samples. The sensitivity is normalized to the highest value. The measurement uncertainties were estimated in the order of ± 10%, similarly to what has been reported by Wei et al. [33]; this leads to an uncertainty for the sensitivity of 15%.

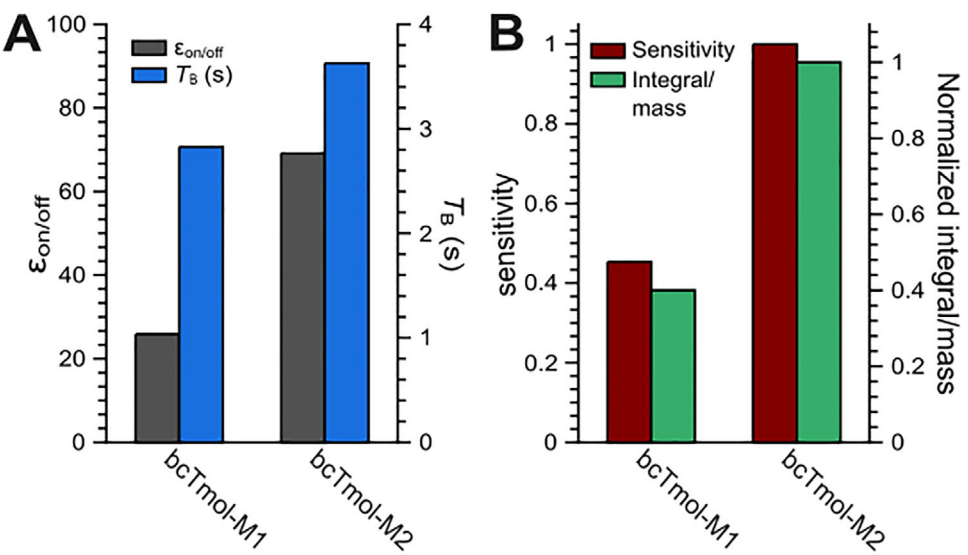

FIGURE 6 | DNP performance of bcTmol-M1 and bcTmol-M2 (10 mM, ethylene-glycol/H_2O (3/7 v/v)) at 14.1 T and 100 K. (A) The enhancement ($\epsilon_{on/off}$) and the buildup time (T_B). (B) Sensitivity and normalized integrals. Normalized integral/mass refers to the integrated NMR signal, divided by the mass of the sample packed in the rotor, allowing comparison of the absolute signal obtained per unit mass across samples. The sensitivity is normalized to the highest value. The measurement uncertainties were estimated in the order of ± 10%, similarly to what has been reported by Wei et al. [33]; this leads to an uncertainty for the sensitivity of 15%.

and evaluated their DNP performance at 14.1 T. The bcTCOOKs demonstrated excellent aqueous solubility, while the bcTmols were unexpectedly poorly water-soluble. The DNP performance of bcTCOOKs was compared to the well-established polarizing agents, bcTol, bcTol-M, and AsymPol-POK. Both bcTCOOK and bcTCOOK-M2 demonstrated higher DNP enhancement than its structural analogues bcTol and bcTol-M, respectively. However, bcTCOOK-M1 showed slightly lower DNP performance than reported for the singly *N*-alkylated AMUPol. The EPR measurements and DFT simulations were in agreement with the observed

DNP results: an increasing number of *N*-methyl substituents improved the relative *g*-tensor orientation and strengthened the electron–electron coupling (*J*), leading to higher polarization efficiency and shorter buildup times. Overall, bcTCOOK-M2 emerged as the most promising polarizing agent, due to its high solubility in aqueous solutions, fast buildup time, and high DNP sensitivity, making it competitive with AsymPol-POK at 14.1 T and 100 K. Importantly, the synthesis of bcTCOOK-M2 was significantly higher yielding and easier to perform than for bcTol-M and AsymPol-POK. Thus, bcTCOOK-M2 is an excellent candidate for routine DNP-NMR applications in highly polar solvents.

Acknowledgments

The National High Magnetic Field Laboratory (NHMFL) is funded by the National Science Foundation Division of Materials Research (DMR-2128556) and the State of Florida. A portion of this work was supported by National Institutes of Health Grant RM1 GM148766. This project has received partial support from the European Union's Horizon 2020 research and Innovation Programme under Grant Agreement 101008500 (PANACEA). This work was also supported by the Icelandic Research Fund (Grant 239662) and the University of Iceland Research Fund (S.Th.S.), as well as a doctoral fellowship from the University of Iceland Research Fund (A.T.W.). The authors thank Dr. S. Jonsdottir and Dr. Gunnar W. Reginsson for assistance with collecting analytical data for structural characterization of new compounds and members of the Sigurdsson research group for helpful discussions.

Funding

This study was supported by Horizon 2020 Framework Programme (Grants 101008500).

Conflicts of Interest

The authors declare no conflicts of interest.

Data Availability Statement

The data that support the findings of this study are openly available in Zenodo at https://doi.org/10.5281/zenodo.19207447, reference number 19207447.

References

1. B. Reif, S. E. Ashbrook, L. Emsley, and M. Hong, "Solid-State NMR Spectroscopy," *Nature Reviews Methods Primers* 1 (2021): 2, https://doi.org/10.1038/s43586-020-00002-1.

2. B. Plainchont, P. Berruyer, J. N. Dumez, S. Jannin, and P. Giraudeau, "Dynamic Nuclear Polarization Opens New Perspectives for NMR Spectroscopy in Analytical Chemistry," *Analytical Chemistry* 90 (2018): 3639–3650, https://doi.org/10.1021/acs.analchem.7b05236.

3. A. W. Overhauser, "Polarization of Nuclei in Metals," *Physical Review* 92 (1953): 411–415, https://doi.org/10.1103/PhysRev.92.411.

4. T. R. Carver and C. P. Slichter, "Polarization of Nuclear Spins in Metals," *Physical Review* 92 (1953): 212–213, https://doi.org/10.1103/PhysRev.92.212.2.

5. Q. Z. Ni, E. Daviso, T. V. Can, et al., "High Frequency Dynamic Nuclear Polarization," *Accounts of Chemical Research* 46 (2013): 1933–1941, https://doi.org/10.1021/ar300348n.

6. A. S. Lilly Thankamony, J. J. Wittmann, M. Kaushik, and B. Corzilius, "Dynamic Nuclear Polarization for Sensitivity Enhancement in Modern Solid-State NMR," *Progress in Nuclear Magnetic Resonance Spectroscopy* 102–103 (2017): 120–195, https://doi.org/10.1016/j.pnmrs.2017.06.002.

7. B. Corzilius, A. A. Smith, and R. G. Griffin, "Solid Effect in Magic Angle Spinning Dynamic Nuclear Polarization," *Journal of chemical physics* 137 (2012): 054201, https://doi.org/10.1063/1.4738761.

8. K. R. Thurber and R. Tycko, "Theory for Cross Effect Dynamic Nuclear Polarization Under Magic-Angle Spinning in Solid State Nuclear Magnetic Resonance: The Importance of Level Crossings," *Journal of Chemical Physics* 137 (2012): 084508, https://doi.org/10.1063/1.4747449.

9. F. Mentink-Vigier, U. Akbey, Y. Hovav, S. Vega, H. Oschkinat, and A. Feintuch, "Fast Passage Dynamic Nuclear Polarization on Rotating Solids," *Journal of Magnetic Resonance* 224 (2012): 13–21, https://doi.org/10.1016/j.jmr.2012.08.013.

10. R. Wei, Y. Rao, A. Venkatesh, and L. Emsley, "Solid Effect Dynamic Nuclear Polarization Enhancement of >500 at 9.4 T," *Journal of Physical Chemistry Letters* 15 (2024): 12408–12415, https://doi.org/10.1021/acs.jpclett.4c03147.

11. K.-N. Hu, H.-H. Yu, T. M. Swager, and R. G. Griffin, "Dynamic Nuclear Polarization With Biradicals," *Journal of the American Chemical Society* 126 (2004): 10844–10845, https://doi.org/10.1021/ja039749a.

12. K. N. Hu, G. T. Debelouchina, A. A. Smith, and R. G. Griffin, "Quantum Mechanical Theory of Dynamic Nuclear Polarization in Solid Dielectrics," *Journal of Chemical Physics* 134 (2011): 125105, https://doi.org/10.1063/1.3564920.

13. A. Equbal, A. Leavesley, S. K. Jain, and S. Han, "Cross-Effect Dynamic Nuclear Polarization Explained: Polarization, Depolarization, and Oversaturation," *Journal of Physical Chemistry Letters* 10 (2019): 548–558, https://doi.org/10.1021/acs.jpclett.8b02834.

14. S. Hediger, D. Lee, F. Mentink-Vigier, and G. De Paëpe, "MAS-DNP Enhancements: Hyperpolarization, Depolarization, and Absolute Sensitivity," *eMagRes* 7 (2018): 105–116, https://doi.org/10.1002/9780470034590.emrstm1559.

15. T. V. Can, M. A. Caporini, F. Mentink-Vigier, et al., "Overhauser Effects in Insulating Solids," *Journal of Chemical Physics* 141 (2014): 064202, https://doi.org/10.1063/1.4891866.

16. M. Lelli, S. R. Chaudhari, D. Gajan, et al., "Solid-State Dynamic Nuclear Polarization at 9.4 and 18.8 T From 100 K to Room Temperature," *Journal of the American Chemical Society* 137 (2015): 14558–14561, https://doi.org/10.1021/jacs.5b08423.

17. L. Delage-Laurin, R. S. Palani, N. Golota, et al., "Overhauser Dynamic Nuclear Polarization With Selectively Deuterated BDPA Radicals," *Journal of the American Chemical Society* 143 (2021): 20281–20290, https://doi.org/10.1021/jacs.1c09406.

18. Z. Miao, F. J. Scott, J. van Tol, C. R. Bowers, A. S. Veige, and F. Mentink-Vigier, "Soliton Based Dynamic Nuclear Polarization: An Overhauser Effect in Cyclic Polyacetylene at High Field and Room Temperature," *Journal of Physical Chemistry Letters* 15 (2024): 3369–3375, https://doi.org/10.1021/acs.jpclett.3c03591.

19. T. Maly, G. T. Debelouchina, V. S. Bajaj, et al., "Dynamic Nuclear Polarization at High Magnetic Fields," *Journal of Chemical Physics* 128 (2008): 052211, https://doi.org/10.1063/1.2833582.

20. W. T. Wenckebach, "Dynamic Nuclear Polarization via the Cross Effect and Thermal Mixing: A. The Role of Triple Spin Flips," *Journal of Magnetic Resonance* 299 (2019): 124–134, https://doi.org/10.1016/j.jmr.2018.12.018.

21. W. T. Wenckebach, "Dynamic Nuclear Polarization via the Cross Effect and Thermal Mixing: B. Energy Transport," *Journal of Magnetic Resonance* 299 (2019): 151–167, https://doi.org/10.1016/j.jmr.2018.12.020.

22. A. Karabanov, G. Kwiatkowski, C. U. Perotto, et al., "Dynamic Nuclear Polarisation by Thermal Mixing: Quantum Theory and Macroscopic Simulations," *Physical Chemistry Chemical Physics* 18 (2016): 30093–30104, https://doi.org/10.1039/c6cp04345c.

23. F. Mentink-Vigier, S. Vega, and G. De Paepe, "Fast and Accurate MAS-DNP Simulations of Large Spin Ensembles," *Physical Chemistry Chemical Physics* 19 (2017): 3506–3522, https://doi.org/10.1039/c6cp07881h.

24. F. Mentink-Vigier, I. Marin-Montesinos, A. P. Jagtap, et al., "Computationally Assisted Design of Polarizing Agents for Dynamic Nuclear Polarization Enhanced NMR: The AsymPol Family," *Journal of the American Chemical Society* 140 (2018): 11013–11019, https://doi.org/10.1021/jacs.8b04911.

25. F. Mentink-Vigier, U. Akbey, H. Oschkinat, S. Vega, and A. Feintuch, "Theoretical Aspects of Magic Angle Spinning—Dynamic Nuclear Polarization," *Journal of Magnetic Resonance* 258 (2015): 102–120, https://doi.org/10.1016/j.jmr.2015.07.001.

26. M. A. Geiger, A. P. Jagtap, M. Kaushik, et al., "Efficiency of Water-Soluble Nitroxide Biradicals for Dynamic Nuclear Polarization in Rotating Solids at 9.4 T: BcTol-M and Cyolyl-TOTAPOL as New Polarizing Agents," *Chemistry–A European Journal* 24 (2018): 13485–13494, https://doi.org/10.1002/chem.201801251.

27. A. Lund, G. Casano, G. Menzildjian, et al., "TinyPols: A Family of Water-Soluble Binitroxides Tailored for Dynamic Nuclear Polarization Enhanced NMR Spectroscopy at 18.8 and 21.1 T," *Chemical Science* 11 (2020): 2810–2818, https://doi.org/10.1039/c9sc05384k.

28. C. Sauvee, G. Casano, S. Abel, et al., "Tailoring of Polarizing Agents in the bTurea Series for Cross-Effect Dynamic Nuclear Polarization in Aqueous Media," *Chemistry–A European Journal* 22 (2016): 5598–5606, https://doi.org/10.1002/chem.201504693.

29. A. Venkatesh, G. Casano, R. Wei, et al., "Rational Design of Dinitroxide Polarizing Agents for Dynamic Nuclear Polarization to Enhance Overall NMR Sensitivity," *Angewandte Chemie International Edition* 63 (2024): e202317337, https://doi.org/10.1002/anie.202317337.

30. F. Mentink-Vigier, A. L. Barra, J. van Tol, S. Hediger, D. Lee, and G. De Paepe, "De Novo Prediction of Cross-Effect Efficiency for Magic Angle Spinning Dynamic Nuclear Polarization," *Physical Chemistry Chemical Physics* 21 (2019): 2166–2176, https://doi.org/10.1039/c8cp06819d.

31. F. Mentink-Vigier, "Optimizing Nitroxide Biradicals for Cross-Effect MAS-DNP: The Role of *g*-Tensors' Distance," *Physical Chemistry Chemical Physics* 22 (2020): 3643–3652, https://doi.org/10.1039/c9cp06201g.

32. R. Harrabi, T. Halbritter, F. Aussenac, et al., "Highly Efficient Polarizing Agents for MAS-DNP of Proton-Dense Molecular Solids," *Angewandte Chemie International Edition* 61 (2022): e202114103, https://doi.org/10.1002/anie.202114103.

33. R. Wei, G. Casano, Y. Zhang, et al., "Systematic Evaluation of Polarizing Agents for Dynamic Nuclear Polarization Enhanced NMR," *Angewandte Chemie International Edition* 64 (2025): e202505944, https://doi.org/10.1002/anie.202505944.

34. F. A. Perras, A. Sadow, and M. Pruski, "Silico Design of DNP Polarizing Agents: Can Current Dinitroxides Be Improved?" *ChemPhysChem* 18 (2017): 2279–2287, https://doi.org/10.1002/cphc.201700299.

35. A. Venkatesh, G. Casano, Y. Rao, et al., "Deuterated TEKPol Biradicals and the Spin-Diffusion Barrier in MAS DNP," *Angewandte Chemie International Edition* 62 (2023): e202304844, https://doi.org/10.1002/anie.202304844.

36. S. Chatterjee, F. J. Scott, S. T. Sigurdsson, A. Venkatesh, and F. Mentink-Vigier, "Indirect Detection of the Protons in and Around Biradicals and Their Mechanistic Role in MAS-DNP," *Journal of Physical Chemistry Letters* 16 (2025): 635–641, https://doi.org/10.1021/acs.jpclett.4c03254.

37. K.-N. Hu, C. Song, H.-H. Yu, T. M. Swager, and R. G. Griffin, "High-Frequency Dynamic Nuclear Polarization Using Biradicals: A Multifrequency EPR Lineshape Analysis," *Journal of Chemical Physics* 128 (2008): 052302, https://doi.org/10.1063/1.2816783.

38. Y. Matsuki, T. Maly, O. Ouari, et al., "Dynamic Nuclear Polarization With a Rigid Biradical," *Angewandte Chemie International Edition* 48 (2009): 4996–5000, https://doi.org/10.1002/anie.200805940.

39. C. Sauvee, M. Rosay, G. Casano, et al., "Highly Efficient, Water-Soluble Polarizing Agents for Dynamic Nuclear Polarization at High Frequency," *Angewandte Chemie International Edition* 52 (2013): 10858–10861, https://doi.org/10.1002/anie.201304657.

40. A. Zagdoun, G. Casano, O. Ouari, et al., "Large Molecular Weight Nitroxide Biradicals Providing Efficient Dynamic Nuclear Polarization at Temperatures up to 200 K," *Journal of the American Chemical Society* 135 (2013): 12790–12797, https://doi.org/10.1021/ja405813t.

41. A. P. Jagtap, M. A. Geiger, D. Stoppler, M. Orwick-Rydmark, H. Oschkinat, and S. T. Sigurdsson, "bcTol: A Highly Water-Soluble Biradical for Efficient Dynamic Nuclear Polarization of Biomolecules," *Chemical Communications* 52 (2016): 7020–7023, https://doi.org/10.1039/c6cc01813k.

42. L. Niccoli, G. Casano, G. Menzildjian, et al., "Efficient DNP at High Fields and Fast MAS With Antenna-Sensitized Dinitroxides," *Chemical Science* 15 (2024): 16582–16593, https://doi.org/10.1039/d4sc04473h.

43. A. Zagdoun, G. Casano, O. Ouari, et al., "A Slowly Relaxing Rigid Biradical for Efficient Dynamic Nuclear Polarization Surface-Enhanced NMR Spectroscopy: Expeditious Characterization of Functional Group Manipulation in Hybrid Materials," *Journal of the American Chemical Society* 134 (2012): 2284–2291, https://doi.org/10.1021/ja210177v.

44. X. Cai, A. Lucini Paioni, A. Adler, et al., "Highly Efficient Trityl-Nitroxide Biradicals for Biomolecular High-Field Dynamic Nuclear Polarization," *Chemistry* 27 (2021): 12758–12762, https://doi.org/10.1002/chem.202102253.

45. T. Halbritter, R. Harrabi, S. Paul, et al., "PyrroTriPol: A Semi-Rigid Trityl-Nitroxide for High Field Dynamic Nuclear Polarization," *Chemical Science* 14 (2023): 3852–3864, https://doi.org/10.1039/d2sc05880d.

46. R. Yao, D. Beriashvili, W. Zhang, et al., "Hydrophilic and Rigidly Linked Trityl-Nitroxide Biradicals for Cellular High-Field Dynamic Nuclear Polarization," *Chemical Science* 13 (2022): 14157–14164, https://doi.org/10.1039/d2sc04668g.

47. D. Wisser, G. Karthikeyan, A. Lund, et al., "BDPA-Nitroxide Biradicals Tailored for Efficient Dynamic Nuclear Polarization Enhanced Solid-State NMR at Magnetic Fields up to 21.1 T," *Journal of the American Chemical Society* 140 (2018): 13340–13349, https://doi.org/10.1021/jacs.8b08081.

48. X. Du, Z. Huang, Q. Shao, et al., "Acrylamide-Linked Water-Soluble Nitroxide Biradicals With Enhanced Electron–Electron Couplings for Dynamic Nuclear Polarization at 14.1 T," *Journal of Physical Chemistry Letters* 16 (2025): 9217–9226, https://doi.org/10.1021/acs.jpclett.5c01749.

49. D. J. Kubicki, G. Casano, M. Schwarzwalder, et al., "Rational Design of Dinitroxide Biradicals for Efficient Cross-Effect Dynamic Nuclear Polarization," *Chemical Science* 7 (2016): 550–558, https://doi.org/10.1039/c5sc02921j.

50. F. Mentink-Vigier, T. Dubroca, J. Van Tol, and S. T. Sigurdsson, "The Distance Between *g*-Tensors of Nitroxide Biradicals Governs MAS-DNP Performance: The Case of the bTurea Family," *Journal of Magnetic Resonance* 329 (2021): 107026, https://doi.org/10.1016/j.jmr.2021.107026.

51. S. Stoll and A. Schweiger, "EasySpin, a Comprehensive Software Package for Spectral Simulation and Analysis in EPR," *Journal of Magnetic Resonance* 178 (2006): 42–55, https://doi.org/10.1016/j.jmr.2005.08.013.

52. J. A. Weil and J. R. Bolton, "Systems with More than One Unpaired Electron," in *Electron Paramagnetic Resonance: Elementary Theory and Practical Applications*, 2nd ed. (Wiley Inc, 2006), 158–207, https://doi.org/10.1002/9780470084984.ch6.

53. J. Soetbeer, P. Gast, J. J. Walish, et al., "Conformation of Bis-Nitroxide Polarizing Agents by Multi-Frequency EPR Spectroscopy," *Physical Chemistry Chemical Physics* 20 (2018): 25506–25517, https://doi.org/10.1039/c8cp05236k.

54. C. Bannwarth, E. Caldeweyher, S. Ehlert, et al., "Extended Tight-Binding Quantum Chemistry Methods," *WIREs Computational Molecular Science* 11 (2020): e1493, https://doi.org/10.1002/wcms.1493.

55. P. Pracht, F. Bohle, and S. Grimme, "Automated Exploration of the Low-Energy Chemical Space With Fast Quantum Chemical Methods," *Physical Chemistry Chemical Physics* 22 (2020): 7169–7192, https://doi.org/10.1039/c9cp06869d.

56. G. Stevanato, G. Casano, D. J. Kubicki, et al., "Open and Closed Radicals: Local Geometry Around Unpaired Electrons Governs Magic-Angle Spinning Dynamic Nuclear Polarization Performance," *Journal of the American Chemical Society* 142 (2020): 16587–16599, https://doi.org/10.1021/jacs.0c04911.

57. K. Tagami, A. Equbal, I. Kaminker, B. Kirtman, and S. Han, "Biradical Rotamer States Tune Electron J Coupling and MAS Dynamic Nuclear Polarization Enhancement," *Solid State Nuclear Magnetic Resonance* 101 (2019): 12–20, https://doi.org/10.1016/j.ssnmr.2019.04.002.

58. S. Chatterjee, A. Venkatesh, S. T. Sigurdsson, and F. Mentink-Vigier, "Role of Protons in and around Strongly Coupled Nitroxide Biradicals for Cross-Effect Dynamic Nuclear Polarization," *Journal of Physical Chemistry Letters* 15 (2024): 2160–2168, https://doi.org/10.1021/acs.jpclett.3c03472.

59. F. J. Scott, S. Eddy, T. Gullion, and F. Mentink-Vigier, "Sorbitol-Based Glass Matrices Enable Dynamic Nuclear Polarization beyond 200 K," *Journal of Physical Chemistry Letters* 15 (2024): 8743–8751, https://doi.org/10.1021/acs.jpclett.4c02054.

60. K. R. Thurber and R. Tycko, "Perturbation of Nuclear Spin Polarizations in Solid State NMR of Nitroxide-Doped Samples by Magic-Angle Spinning without Microwaves," *Journal of Chemical Physics* 140 (2014): 184201, https://doi.org/10.1063/1.4874341.

61. F. Mentink-Vigier, S. Paul, D. Lee, et al., "Nuclear Depolarization and Absolute Sensitivity in Magic-Angle Spinning Cross Effect Dynamic Nuclear Polarization," *Physical Chemistry Chemical Physics* 17 (2015): 21824–21836, https://doi.org/10.1039/c5cp03457d.

62. B. Corzilius, L. B. Andreas, A. A. Smith, Q. Z. Ni, and R. G. Griffin, "Paramagnet Induced Signal Quenching in MAS-DNP Experiments in Frozen Homogeneous Solutions," *Journal of Magnetic Resonance* 240 (2014): 113–123, https://doi.org/10.1016/j.jmr.2013.11.013.

63. T. Kobayashi, O. Lafon, A. S. Thankamony, et al., "Analysis of Sensitivity Enhancement by Dynamic Nuclear Polarization in Solid-State NMR: A Case Study of Functionalized Mesoporous Materials," *Physical Chemistry Chemical Physics* 15 (2013): 5553–5562, https://doi.org/10.1039/c3cp00039g.

64. A. J. Rossini, A. Zagdoun, M. Lelli, et al., "One Hundred Fold Overall Sensitivity Enhancements for Silicon-29 NMR Spectroscopy of Surfaces by Dynamic Nuclear Polarization With CPMG Acquisition," *Chemical Science* 3 (2012): 108–115, https://doi.org/10.1039/c1sc00550b.

65. H. Takahashi, C. Fernandez-de-Alba, D. Lee, et al., "Optimization of an Absolute Sensitivity in a Glassy Matrix during DNP-Enhanced Multidimensional Solid-State NMR Experiments," *Journal of Magnetic Resonance* 239 (2014): 91–99, https://doi.org/10.1016/j.jmr.2013.12.005.

66. S. Lange, A. H. Linden, U. Akbey, et al., "The Effect of Biradical Concentration on the Performance of DNP-MAS-NMR," *Journal of Magnetic Resonance* 216 (2012): 209–212, https://doi.org/10.1016/j.jmr.2012.01.002.

67. N. A. Prisco, A. C. Pinon, L. Emsley, and B. F. Chmelka, "Scaling Analyses for Hyperpolarization Transfer across a Spin-Diffusion Barrier and Into Bulk Solid Media," *Physical Chemistry Chemical Physics* 23 (2021): 1006–1020, https://doi.org/10.1039/d0cp03195j.

68. M. D. Hanwell, D. E. Curtis, D. C. Lonie, T. Vandermeersch, E. Zurek, and G. R. Hutchison, "Avogadro: An Advanced Semantic Chemical Editor, Visualization, and Analysis Platform," *Journal of Cheminformatics* 4 (2012): 17, https://doi.org/10.1186/1758-2946-4-17.

69. K. Sharkey, M. D. Hanwell, C. Harris, and A. Vacanti, "Avogadro 2 and Open Chemistry, Kitware Blog," (2013), https://www.kitware.com/avogadro-2-and-open-chemistry/.

70. C. Bannwarth, S. Ehlert, and S. Grimme, "GFN2-xTB-An Accurate and Broadly Parametrized Self-Consistent Tight-Binding Quantum Chemical Method With Multipole Electrostatics and Density-Dependent Dispersion Contributions," *Journal of Chemical Theory and Computation* 15 (2019): 1652–1671, https://doi.org/10.1021/acs.jctc.8b01176.

71. S. Ehlert, M. Stahn, S. Spicher, and S. Grimme, "Robust and Efficient Implicit Solvation Model for Fast Semiempirical Methods," *Journal of Chemical Theory and Computation* 17 (2021): 4250–4261, https://doi.org/10.1021/acs.jctc.1c00471.

72. F. Neese, "The ORCA Program System," *WIREs Computational Molecular Science* 2 (2011): 73–78, https://doi.org/10.1002/wcms.81.

73. F. Neese, "Software Update: The ORCA Program System—Version 6.0," *WIREs Computational Molecular Science* 15 (2025): e70019, https://doi.org/10.1002/wcms.70019.

74. S. Grimme, A. Hansen, S. Ehlert, and J. M. Mewes, "SCAN-3c: A "Swiss Army Knife" Composite Electronic-Structure Method," *Journal of Chemical Physics* 154 (2021): 064103, https://doi.org/10.1063/5.0040021.

75. R. Harrabi, T. Halbritter, S. Alarab, et al., "AsymPol-TEKs as Efficient Polarizing Agents for MAS-DNP in Glass Matrices of Non-Aqueous Solvents," *Physical Chemistry Chemical Physics* 26 (2024): 5669–5682, https://doi.org/10.1039/d3cp04271e.

76. B. M. Fung, A. K. Khitrin, and K. Ermolaev, "An Improved Broadband Decoupling Sequence for Liquid Crystals and Solids," *Journal of Magnetic Resonance* 142 (2000): 97–101, https://doi.org/10.1006/jmre.1999.1896.

77. T. Dubroca, A. N. Smith, K. J. Pike, et al., "A Quasi-Optical and Corrugated Waveguide Microwave Transmission System for Simultaneous Dynamic Nuclear Polarization NMR on Two Separate 14.1 T Spectrometers," *Journal of Magnetic Resonance* 289 (2018): 35–44, https://doi.org/10.1016/j.jmr.2018.01.015.

Supporting Information

Additional supporting information can be found online in the Supporting Information section.

The authors have cited additional references within the Supporting Information [68–77].

Supporting File 1: chem71632-sup-0001-SuppMat.pdf